



Impaired Hippocampal Neurovascular Coupling in a Mouse Model of Alzheimer's Disease

Lin Li^{1,2}, Xin-Kang Tong³, Mohammadamin Hosseini Kahnouei^{1,2,4}, Diane Vallerand^{1,4}, Edith Hamel³ and H  l  ne Girouard^{1,2,4,5*}

¹ Department of Pharmacology and Physiology, Faculty of Medicine, Universit   de Montr  al, Montr  al, QC, Canada,

² Groupe de Recherche sur le Syst  me Nerveux Central (GRSNC), Universit   de Montr  al, Montr  al, QC, Canada,

³ Laboratory of Cerebrovascular Research, Montreal Neurological Institute, McGill University, Montr  al, QC, Canada,

⁴ Centre Interdisciplinaire de Recherche sur le Cerveau et l'Apprentissage (CIRCA), Universit   de Montr  al, Montr  al, QC, Canada, ⁵ Centre de Recherche de l'Institut Universitaire de G  riatrie de Montr  al, Montr  al, QC, Canada

OPEN ACCESS

Edited by:

Fabrice Dabertrand,
University of Colorado School of
Medicine, United States

Reviewed by:

Osama F. Harraz,
University of Vermont, United States
Craig Edward Brown,
University of Victoria, Canada

*Correspondence:

H  l  ne Girouard
helene.girouard@umontreal.ca

Specialty section:

This article was submitted to
Vascular Physiology,
a section of the journal
Frontiers in Physiology

Received: 27 May 2021

Accepted: 02 July 2021

Published: 12 August 2021

Citation:

Li L, Tong X-K, Hosseini Kahnouei M, Vallerand D, Hamel E and Girouard H (2021) Impaired Hippocampal Neurovascular Coupling in a Mouse Model of Alzheimer's Disease. *Front. Physiol.* 12:715446. doi: 10.3389/fphys.2021.715446

Alzheimer's disease (AD), the most common form of dementia, is characterized by neuronal degeneration and cerebrovascular dysfunction. Increasing evidence indicates that cerebrovascular dysfunction may be a key or an aggravating pathogenic factor in AD. This emphasizes the importance to investigate the tight coupling between neuronal activity and cerebral blood flow (CBF) termed neurovascular coupling (NVC). NVC depends on all cell types of the neurovascular unit within which astrocytes are important players in the progression of AD. Hence, the objective of this study was to characterize the hippocampal NVC in a mouse model of AD. Hippocampal NVC was studied in 6-month-old amyloid-beta precursor protein (APP) transgenic mice and their corresponding wild-type littermates using *in vivo* laser Doppler flowmetry to measure CBF in area CA1 of the hippocampus in response to Schaffer collaterals stimulation. *Ex vivo* two-photon microscopy experiments were performed to determine astrocytic Ca²⁺ and vascular responses to electrical field stimulation (EFS) or caged Ca²⁺ photolysis in hippocampal slices. Neuronal synaptic transmission, astrocytic endfeet Ca²⁺ in correlation with reactive oxygen species (ROS), and vascular reactivity in the presence or absence of Tempol, a mimetic of superoxide dismutase, were further investigated using electrophysiological, caged Ca²⁺ photolysis or pharmacological approaches. Whisker stimulation evoked-CBF increases and *ex vivo* vascular responses to EFS were impaired in APP mice compared with their age-matched controls. APP mice were also characterized by decreased basal synaptic transmission, a shorter astrocytic Ca²⁺ increase, and altered vascular response to elevated perivascular K⁺. However, long-term potentiation, astrocytic Ca²⁺ amplitude in response to EFS, together with vascular responses to nitric oxide remained unchanged. Importantly, we found a significantly increased Ca²⁺ uncaging-induced ROS production in APP mice. Tempol prevented the vascular response impairment while normalizing astrocytic Ca²⁺ in APP

mice. These findings suggest that NVC is altered at many levels in APP mice, at least in part through oxidative stress. This points out that therapies against AD should include an antioxidative component to protect the neurovascular unit.

Keywords: neurovascular coupling, Alzheimer's disease, hippocampus, astrocyte, two-photon imaging

INTRODUCTION

Alzheimer's disease (AD), the most common form of dementia in the elderly, is characterized by progressive memory decline and deficits. The disease is defined by pathological features such as amyloid β accumulation, hyperphosphorylated tau protein in the form of neurofibrillary tangles, neuronal and synaptic loss, and cerebrovascular dysfunction (Jack et al., 2018). Increasing evidences indicate that cerebrovascular dysfunctions may play a key role in the pathogenesis of AD (Zlokovic, 2011). Since the cerebrovascular deficits develop very early in the AD process, it is detectable in individuals with mild cognitive impairment (MCI) and promote conversion from MCI to AD (Yetkin et al., 2006; Iadecola, 2010; Li et al., 2011). It has been widely reported that neurovascular coupling (NVC), a vasodilatory response to neuronal activity, is impaired in AD patients or animal models (Hock et al., 1997; Iadecola, 2004; Tong et al., 2012; Lourenço et al., 2017). However, the underlying mechanisms of NVC dysfunction in the context of AD are still largely unknown.

NVC depends on all the components of the neurovascular unit, which comprises neurons, astrocytes, and vascular cells. Astrocytes are recognized to transduce the neuronal signal into a dynamic intracellular calcium (Ca^{2+}) signal, which travels to astrocytic processes ("endfeet") to modulate local blood flow (Zonta et al., 2003a; Filosa et al., 2004; Mulligan and MacVicar, 2004; Takano et al., 2006). In murine models of AD, the astrocytic Ca^{2+} signaling is disturbed, with elevated resting Ca^{2+} levels, increased frequency of spontaneous Ca^{2+} spikes or abnormal Ca^{2+} waves (Takano et al., 2007; Kuchibhotla et al., 2009). However, the astrocytic Ca^{2+} signaling in relation to the vascular responses in hippocampal NVC has never been investigated in these models.

Reactive oxygen species (ROS) are elevated in astrocytes of APP mice and $\text{A}\beta$ -induced ROS is known to alter vascular regulation (Abramov et al., 2004; Tong et al., 2009). Furthermore, antioxidant drugs completely rescue cerebrovascular functions in old AD transgenic mice (Nicolakakis et al., 2008). Thus, we hypothesized that ROS, may impair NVC by altering the communication between neurons, astrocytes and vascular cells in AD mice.

In this study we found that hippocampal NVC is altered at many levels in adult APP mice compared with age-matched controls. Indeed, basal synaptic transmission in hippocampus is attenuated, the astrocytic Ca^{2+} response to electrical field stimulation (EFS) is shorter, the CBF response to Schaffer collaterals stimulation is decreased, and the vascular responses to EFS, to Ca^{2+} uncaging or to elevated perivascular K^+ are reversed or attenuated. Importantly, Ca^{2+} uncaging-induced ROS production is elevated in APP mice and ROS scavenging rescue NVC impairment while normalizing astrocytic

Ca^{2+} signaling in these mice. The data unveil impaired hippocampal NVC in APP mice and, further, they reinforce the great potential for antioxidant therapies to protect the neurovascular unit in AD.

MATERIALS AND METHODS

Animals

All experimental protocols used in this study are in accord with the Canadian Council on Animal Care, the ARRIVE (Animal Research: Reporting of *In Vivo* Experiments) guidelines and approved by the Committee on Ethics of Animal Experiments of the Université de Montréal or the Montreal Neurological Institute at McGill University. Heterozygous transgenic C57BL/6 male and female mice of 6 month old carrying the familial Swedish (K670N, M671L; APPSwe) and Indiana (V717F; APPInd) human APP mutations directed by the (platelet-derived growth factor) PDGF-chain promoter (APP mice, J20 line) (Mucke et al., 2000) and their wild-type (WT) littermates were used. Animals were housed 4/cages in a temperature-controlled room with *ad libitum* access to water and a standard protein rodent diet (4% fat, 14% protein rodent maintenance diet, Harlan Teklad global). Mice were randomly separated into different groups for each experiment.

Hippocampal CBF Measurements

Mice (WT, $n = 6$ and APP, $n = 6$) were anesthetized with ketamine (85 mg/kg, i.m.; Bioniche Life Sciences, CAN) and xylazine (3 mg/kg, i.m.; Haver), and placed in a stereotaxic frame on a heating blanket for maintaining body temperature stable at 37°C. CBF increases were measured in the CA1 area of the hippocampus with laser Doppler flowmetry (Transonic Systems, Ithaca, NY, United States) during stimulation of the Schaffer collaterals in the CA3 area (200 Hz, 50 μA , 0.5 ms, 1 s on/1 s off for 20 s isolated pulse stimulator; A-M Systems, Sequim, WA, United States) (Figure 1A). A 1.0 mm laser Doppler probe was positioned over the CA1 area following insertion through the cerebral cortex via a small opening. Stereotaxic coordinates (Franklin and Paxinos, 1997) were as follows: stimulating electrode (angle: 41 degrees, anterior-posterior (AP): Bregma, -2.3 mm; lateral (L): 3.6 mm and dorso-ventral (V): 1.8 mm; Laser Doppler probe, AP: Bregma, -2.3 mm, L: 1.7 mm and V: 1.0 mm). A total of 4–6 stimulations were performed for each mouse and averaged. CBF was recorded and averaged before, during, and after the stimulation. For illustration, curves were generated representing 1 s average of the evoked CBF, expressed as a percentage change from 30 s pre-stimulus baseline. Stimulation-evoked CBF responses were expressed as the percentage change relative to baseline.

Immunohistochemical Stainings

Mice ($n = 4/\text{group}$) were perfused through the heart with a solution of 4% paraformaldehyde (PFA) in 0.1M phosphate buffer, and their brains were removed and post-fixed in the same solution overnight (4°C). Then, brains were cut in the midline, one hemisphere was processed for paraffin sectioning (5 μm -thick coronal sections) and the other was processed for sectioning on a freezing microtome (25 μm -thick sections) collected in PBS, and kept in anti-freezing solution until use. Paraffin-embedded sections were incubated overnight with a rat anti-Ly6c (1:500, abcam, Canada, an endothelial cell marker), or goat anti-collagen IV (1:300, Millipore-Sigma, Oakville, Canada, a marker of vascular basement membrane). The immunoreactive material was visualized with 3, 3'-diaminobenzidine enhanced with nickel (DAB-Ni). The images were captured on a Panoramic slide scanner (MIRAX SCAN, Zeiss, Oberkochen, Germany), and the total surface area and diameter occupied by blood vessel in the whole hippocampus were measured in each section using MetaMorph6.1r3 software (Universal Imaging, Downingtown, PA). The values were transformed as a ratio of the total hippocampal surface area, and then expressed as a percent of WT controls. Freezing microtome sections were used for triple immunostaining of amyloid β (A β) plaques, astrocytes, and blood vessels. The sections were concurrently incubated overnight in rat anti-Ly6c, rabbit anti-GFAP (1:1,000, Dako, Denmark, an astroglial marker) and mouse anti-6E10 (1:1,000, Covance, a marker of A β), and the respective reactions were visualized with species-specific donkey anti-rabbit cyanine 2 (Cy2)-, anti-rat Cy3-, and anti-mouse Cy5-conjugated affiniPure secondary antibodies (Jackson ImmunoResearch, West Grove, PA). The associations of astroglial endfeet with local blood vessels or with A β plaques were visualized by confocal microscopy (Zeiss LSM 510; Zeiss, Jena, Germany) using simultaneous triple-channel detection with emission intensity of 488 nm (AlexaFluor/Cy2), 543 nm (Cy3), and 640 nm (Cy5).

Hippocampal Slice Preparation

Mice were sacrificed and brains were quickly removed and placed into ice-cold cutting artificial CSF (aCSF) (250 mM sucrose, 3 mM KCl, 26 mM NaHCO₃, 1.25 mM NaH₂PO₄, 0.5 mM CaCl₂, 6 mM MgCl₂, 10 mM glucose, and 400 μM L-ascorbic acid, equilibrated with a 95%O₂/5%CO₂ gas at a pH of 7.4). Coronal sections of the hippocampus (180 μm for two-photon imaging or 400 μm for electrophysiological recording) were kept for 20 min at 35°C in recording artificial CSF (125 mM NaCl, 3 mM KCl, 26 mM NaHCO₃, 1.25 mM NaH₂PO₄, 2 mM CaCl₂, 1 mM MgCl₂, 10 mM glucose) bubbled with 95%O₂/5%CO₂.

Two-Photon Imaging of Astrocytic Endfoot Ca²⁺ and Arterioles

Hippocampal slices were incubated at 29°C under constant agitation for 1 h in oxygenated aCSF, with the Ca²⁺ indicator Fluo-4 AM (10 μM ; Invitrogen) or the ROS indicator CM-H₂DCFDA (30 μM , 45 min, 25°C), both in the presence of Cremophor EL [0.005% (v/v); Sigma, Oakville, Canada], and pluronic acid F-127 [0.025% (w/v);

EMD Calbiochem, Gibbstown, NJ, United States]. For Ca²⁺ uncaging experiments, slices were coloaded with the caged Ca²⁺ compound, 1-[4,5-dimethoxy-2-nitrophenyl]-EDTA-AM (DMNP-EDTA-AM, 10 μM ; Interchim) using the same loading conditions.

Imaging was performed with a multiphoton laser scanning upright microscope (BX61WI; Olympus, Tokyo, Japan) coupled to a Ti: Sapphire laser (MaiTai HP DeepSee; Spectra Physics, Santa Clara, CA, United States) and equipped with a 20 \times water immersion objective (0.5 numerical aperture; 5 digital zoom factor). Time-lapse images were acquired using the FV10-ASW software (version 3.0; Olympus, Tokyo, Japan) and displayed the arteriole diameter/morphology as visualized by infrared differential interference contrast (IR-DIC) imaging, simultaneously with the free intracellular Ca²⁺ (Fluo-4 AM) in astrocyte endfeet. Fluo-4 AM was excited at 805 nm by the Ti: sapphire laser (100-fs pulses, 0.5 W) laser and fluorescence emission was collected using a 575/150-nm bandpass filter.

For every experiment, morphological criteria were used to distinguish arterioles from venules and capillaries as described earlier (Girouard et al., 2010). Arterioles located 40–80 μm below the cut surface were selected. At the beginning of each experiment, slices were incubated with the thromboxane A₂ receptor agonist, U46619 (150 nM; 20 min) to pre-constrict arterioles to a physiological level of arteriolar tone. The constriction level was the same in APP and WT mice (**Supplementary Figure 1**). An astrocytic endfoot adjacent to the arteriole was then selected at a focal plane corresponding to the highest Fluo-4 AM fluorescence. Images were processed with the Image J software (v.1.45r for Mac OS, NIH, MD Bethesda, United States) and the arteriole luminal diameter was measured adjacently to the selected endfoot on each image. The distance between two points was calculated from a line perpendicular to the arterial walls. The baseline diameter was obtained from the average of 15–20 successive images preceding stimulations. In some experiments, 10 mM K⁺ or the NO donor, sodium nitroprusside (SNP, 100 μM) were added to the aCSF to determine the vascular reactivity to these vasomediators.

Electrical Field Stimulation of Neuronal Activity and Photolysis of Caged Ca²⁺

Electrical field stimulation (EFS) was used to stimulate neuronal fibers by applying a 50-Hz alternating square pulse of 0.3 ms duration for 2.5 s (50 V) via a concentric bipolar electrode inserted into hippocampal slice near the vessel wall (around 100–150 μm). Multiphoton fluorescence imaging equipped with IR-DIC) microscopy was applied to simultaneously monitor astrocytic endfeet Ca²⁺ (labeled by Fluo4 AM) and arteriolar diameter changes before and after EFS. IR-DIC allowed evaluation of the slice integrity through visualization of dead neurons, which was an exclusion criterion. The elevation of astrocytic [Ca²⁺]_i by EFS was inhibited by tetrodotoxin (Filosa et al., 2004) (data not shown), a blocker of voltage-dependent sodium channels, confirming neuronal involvement. For Ca²⁺ uncaging experiments, the laser was set at 730 nm, which allows for simultaneous excitation of Fluo-4 and photolysis of the caged

Ca^{2+} , DMNP-EDTA (Girouard et al., 2010). A $1.5 \times 1.5 \mu\text{m}$ region of interest (ROI) within an endfoot was scanned at a laser intensity $5 \times$ higher than that used for imaging. Based on our preliminary experiments comparing different laser powers over 30 min, the laser power used for Ca^{2+} imaging was below the threshold for Ca^{2+} uncaging. Reproducible increases in $[\text{Ca}^{2+}]_i$ were detected over multiple uncaging events, and no increases in $[\text{Ca}^{2+}]_i$ were detected in non-loaded slices.

Two-Photon Imaging of Astrocytic Endfoot for ROS Study

ROS production was monitored at 35°C by using the 5-(and-6)-chloromethyl 1-2',7'-dichlorodihydrofluorescein diacetate (CM-H₂DCFDA), a dye sensitive to peroxynitrite 1 (ONOO-), hydrogen peroxide (H₂O₂), and hydroxyl radical (HO[•]; Molecular Probes). CMH₂DCFDA is a non-fluorescent dye until the acetate groups are removed by intracellular esterases and oxidation occurs within the cell. The dye (50 μg) was freshly dissolved each day in 5 μL dimethyl sulfoxide (DMSO). The slices were loaded with 30 μM CM-H₂DCFDA in the dark (45 min; 25°C ; 0.005% [w/v] Pluronic F127). After loading, the slices were washed three times and then kept in aCSF for at least 30 min to ensure deacetylation. Probenecid (1.5 mM) was added to every solution used after loading to inhibit organic anion transporters that remove fluorescent dyes from the cytoplasm. ROS was imaged at 730 nm using the two photon microscope at the same condition as for Ca^{2+} imaging experiments. We assigned the threshold for ROS increases as 1.2 fractional fluorescence (F1/F0).

Endfoot Ca^{2+} and ROS Analysis

F1/F0 values reflect the Ca^{2+} or ROS fluorescence intensity for a ROI in each image (F1) divided by a mean fluorescence value (F0) taken from an average of 15–20 images before stimulation. For some experiments, astrocytic endfoot Ca^{2+} concentrations were determined using the maximal fluorescence method as described earlier (Girouard et al., 2010). To summarize, ionomycin (407950, 10 μM ; EMD Calbiochem) and 20 mM Ca^{2+} were immediately added to aCSF at the end of each experiment to obtain the maximal fluorescence (F_{MAX}). The F_{MAX} value was measured within a ROI (15 \times 15 pixels, or 1.8 \times 1.8 μm) in the selected endfoot. Using this value and experimental parameters, the estimated $[\text{Ca}^{2+}]_i$ was calculated using Maravall's formula (Maravall et al., 2000; Girouard et al., 2010).

Electrophysiology Analysis

After 1 h recovery, the slices were transferred to a recording chamber and perfused continually with the oxygenated aCSF at the temperature of $32 \pm 1^\circ\text{C}$. A glass microelectrode with the resistance of 2–3 M Ω filled with oxygenated aCSF inserted into radiatum layer of CA1 region. Excitatory postsynaptic potential (EPSP) was generated by stimulating the Schaffer collateral pathway using a stimulator (SEN-3301, Nihon Kohden, Japan). Stimulus pulses (0.1 ms duration) were delivered every 15 s. Signals were obtained using an Axoclamp 2B amplifier (Axon Instruments, Foster City, CA, United States), sampled at 20 kHz,

and filtered at 10 kHz, and the output was digitized with a Digidata 1200 converter (Axon Instruments). Stability of baseline recordings was established by delivering single pulses (4/min, 0.1 ms pulse width) for 15 min prior to collection of data. (1) Basal synaptic transmission was assayed by determining input–output relations from extracellular field potential recordings in the stratum radiatum of CA1; the input was the peak amplitude of the fiber volley, and the output was the initial slope of the EPSP. EPSP slopes were evoked by testing stimulation of various intensities (0.1–1.1 mA). (2) Paired-pulse facilitation (PPF) was induced by double stimuli with interpulse interval (IPI) of 25–200 ms. The value of paired-pulse ratio (PPR) is expressed by the second EPSP slope relative to the first EPSP slope. (3) Long-term potentiation (LTP) was induced by four tetani delivered 10 s apart, each at 100 Hz for 1 s after a 20 min baseline period. After delivering tetani, the EPSP slopes were recorded for a further period of 60 min. LTP was determined if the EPSP slopes were larger by 20% compared to the baseline.

Statistical Analysis

All results are presented as mean \pm SEM. Two-way (with repeated measures when appropriate) ANOVA and Bonferroni's multiple comparison test were performed to compare differences among groups. The two-tailed unpaired Student's *t*-test was performed for comparison between two-groups. Differences at $p < 0.05$ were considered statistically significant.

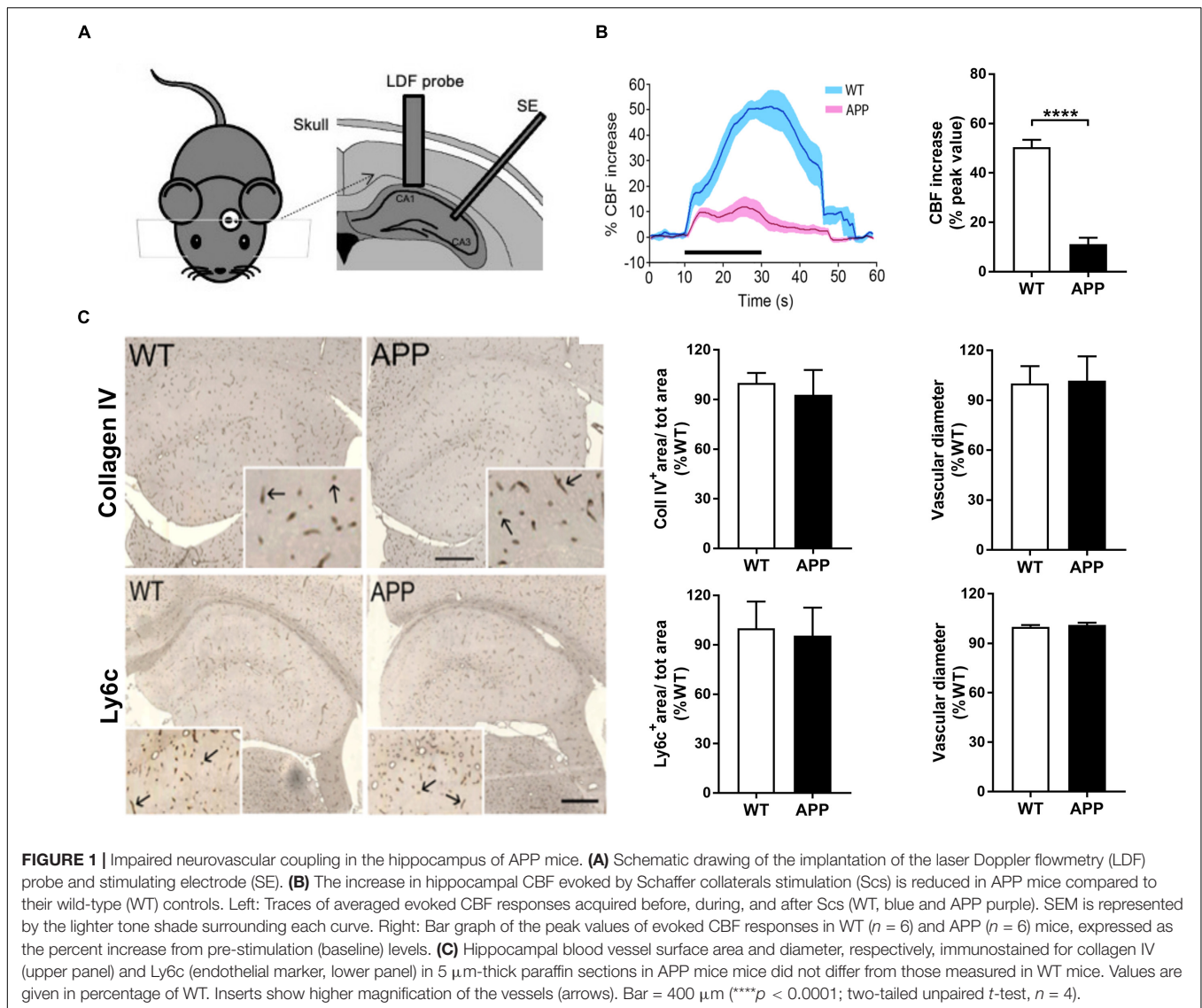
RESULTS

Hippocampal Neurovascular Coupling Is Impaired in APP Mice

We first determined hippocampal CBF increases in response to *in vivo* electrical stimulation of Schaffer collaterals in APP and WT mice. Stimulus-induced hippocampal CBF increase in the CA1 area was significantly reduced in APP mice compared with age-matched WT mice (Figure 1B, $p < 0.0001$), consistent with our previous report of impaired NVC in the cerebral cortex of similarly aged APP mice (Tong et al., 2009).

Vascular loss is a hallmark of the microvascular pathology in AD (Bailey et al., 2004) and may explain, at least in part, the attenuated CBF increase. Staining of vessel basement membrane with collagen IV or endothelial cells with Ly6c showed that both vascular surface area and vessel diameter were comparable between WT and APP mice of the same age (Figure 1C), indicating no apparent vascular density loss or diameter changes in APP mice at that age.

Then, we investigated the mechanisms underlying impaired NVC using acute hippocampal slices. The mean diameter of arterioles at rest was 10.5 μm with a range of 7.5–15 μm . To guarantee that the impaired vascular responses were truly related to EFS in our experimental conditions (33% of experiments using EFS induced neither vascular nor astrocytic endfoot response; data not shown), we defined over 20% increase in Ca^{2+} fluorescence post stimulation as a successful EFS. This threshold was determined from our previous experiments which showed



that the coefficient of variation of resting Ca^{2+} is below 20% (Boily et al., 2021). Imaging in the absence of EFS did not induce any changes in diameter or endfoot Ca^{2+} (Boily et al., 2021).

In addition, 68% (data not shown) of astrocytic endfoot Ca^{2+} increases were accompanied by vascular responses in hippocampal slices of WT mice. EFS that triggered astrocytic endfoot Ca^{2+} increases also induced vascular dilation in both APP and WT mice (Figures 2A,B). In accordance with *in vivo* results, the amplitude of vascular responses to EFS in acute hippocampal slices was significantly reduced in APP mice compared with WT mice (Figure 2C, $p < 0.05$).

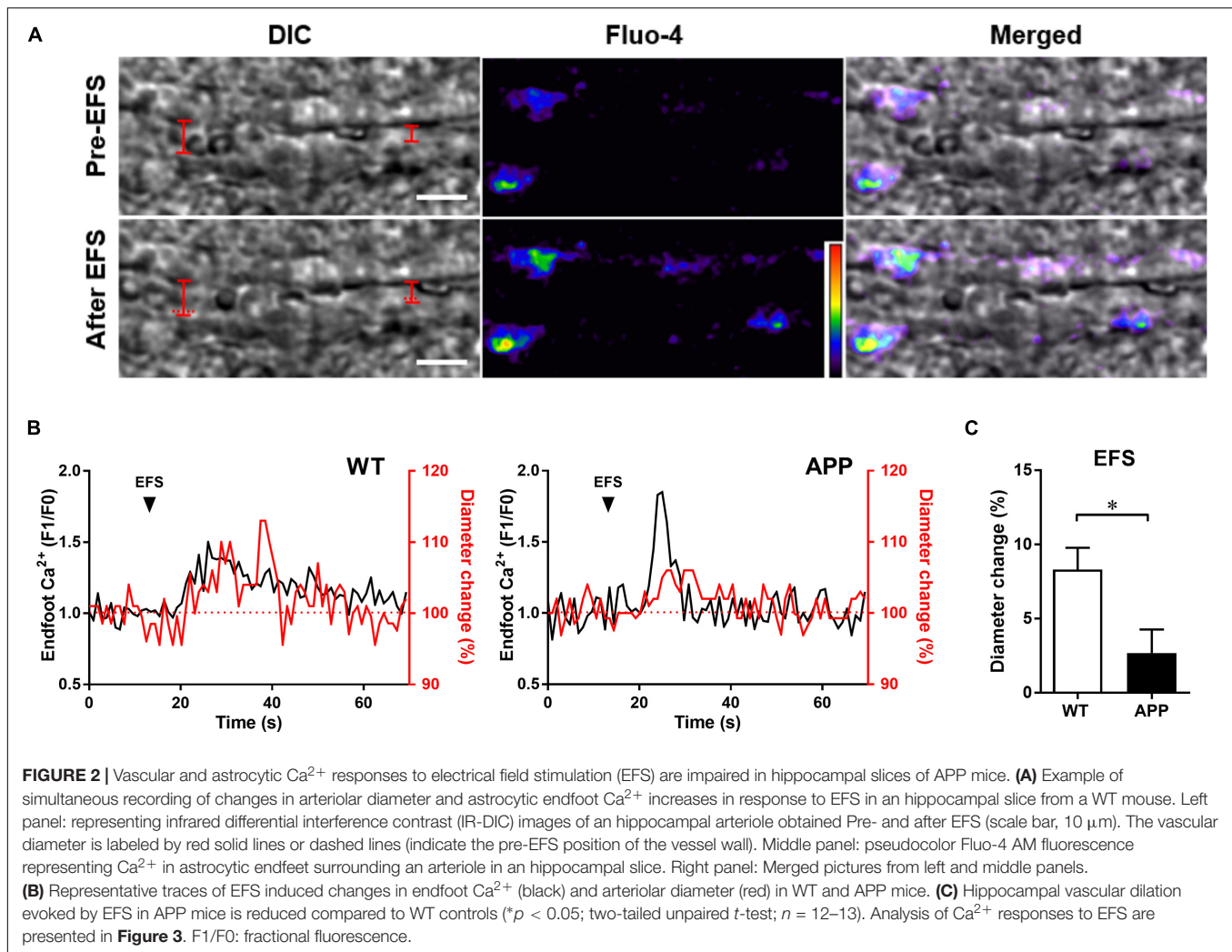
The Astrocytic Endfoot Ca^{2+} Increase in Response to Neuronal Activity Is Attenuated in APP Mice

The resting level of endfoot Ca^{2+} and the amplitude of astrocytic Ca^{2+} responses to EFS were similar in both APP

and WT mice (Figures 3A–D). Neuronal activity-dependent $[\text{Ca}^{2+}]_i$ elevations in astrocytic endfeet occurred within 3 s after the onset of the stimulation and reached a peak after an average of 5.6 ± 0.64 ($n = 15$) and 4.5 ± 0.56 ($n = 13$) s in WT and APP mice, respectively. There was no difference for the period before the onset or peak point of astrocytic Ca^{2+} increases between WT and APP mice. However, the duration of astrocytic endfoot Ca^{2+} elevation was shorter in APP mice compared with WT (Figures 3E,F, $p < 0.01$).

Gliovascular Ca^{2+} Signaling Dependent Pathway Is Impaired in APP Mice

We next asked whether the vascular responses to astrocytic Ca^{2+} increases are impaired in cerebral blood vessels with no apparent vascular amyloidosis from 6-month-old APP mice (Tong et al., 2009). We thus increased astrocytic Ca^{2+} levels

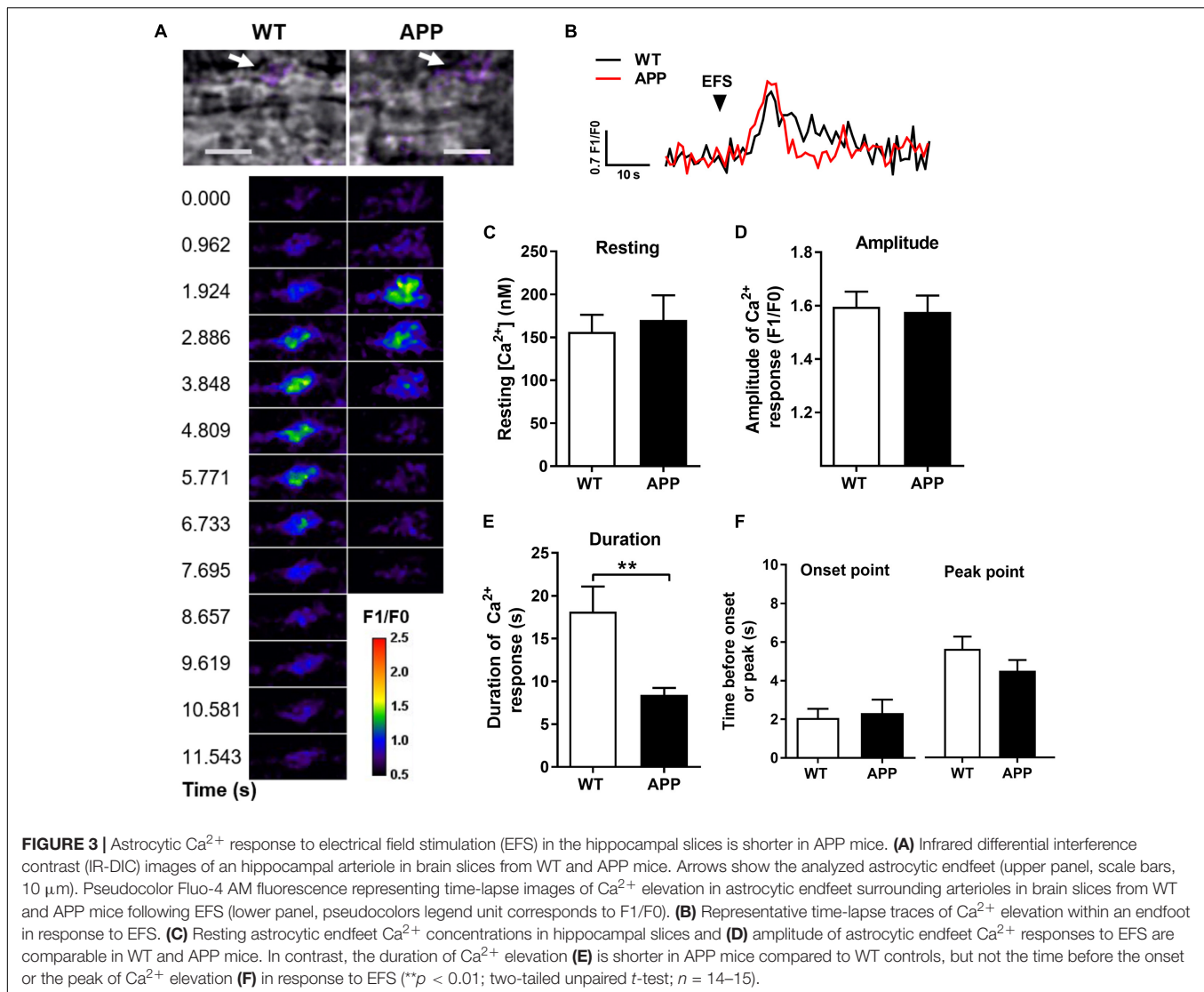


similarly in APP and WT mice using two photon photolysis of caged Ca^{2+} DMNP-EDTA. Uncaging generated modest increase of endfoot Ca^{2+} in a range of 200–600 nM, which are concentrations known to induce arteriolar dilation (Girouard et al., 2010). The Ca^{2+} increase induced by Ca^{2+} uncaging in endfoot was similar in APP and WT mice, showing long lasting elevated Ca^{2+} , but different corresponding vascular responses (**Figures 4A–C**). In the hippocampal slices of APP mice, the arterioles shifted more toward constriction compared with WT mice (**Figure 4D**, $p < 0.05$). This inability to dilate may be explained by a higher level of extracellular perivascular K^+ or attenuated arteriolar dilation response to 10 mM K^+ or to an NO donor in APP mice. Indeed, the vascular responses to K^+ in the presence or absence of the large conductance of Ca^{2+} activated K^+ (BK) channel blocker paxilline were attenuated in APP mice compared to their WT counterpart (**Figure 4E**, $p < 0.05$). In contrast, dilations to the NO donor, SNP, or constrictions to the thromboxane A2 receptor agonist, U46619 were not significantly different in APP mice compared to WT controls (**Figure 4F** and **Supplementary Figure 1**). These data suggest that gliovascular coupling downstream of

astrocytic endfoot Ca^{2+} increase and BK channels is impaired in adult APP mice.

Increased Amplitude of Spontaneous Ca^{2+} Oscillations in Astrocytic Endfeet of APP Mice

The frequency and amplitude of spontaneous astrocytic Ca^{2+} oscillation events may impact Ca^{2+} increases to a stimulus. These events were defined as increases of fluorescence of more than 30% (determined from the coefficient of variability of the baseline intensity) from the baseline intensity ($\Delta\text{F}/\text{F}$). As expected, the maximal and averaged amplitudes of spontaneous Ca^{2+} oscillations in astrocytic endfeet, not their frequency, were significantly increased in APP mice compared with WT mice (**Figure 5**, $p < 0.05$). Since the elevated spontaneous Ca^{2+} oscillation may be due to high levels of A β peptide or A β plaques, we verified whether blood vessel and astrocytic endfeet are located in proximity of A β plaques (**Supplementary Figure 2**).



Impaired Vascular Responses Are Highly Associated With ROS Concentrations

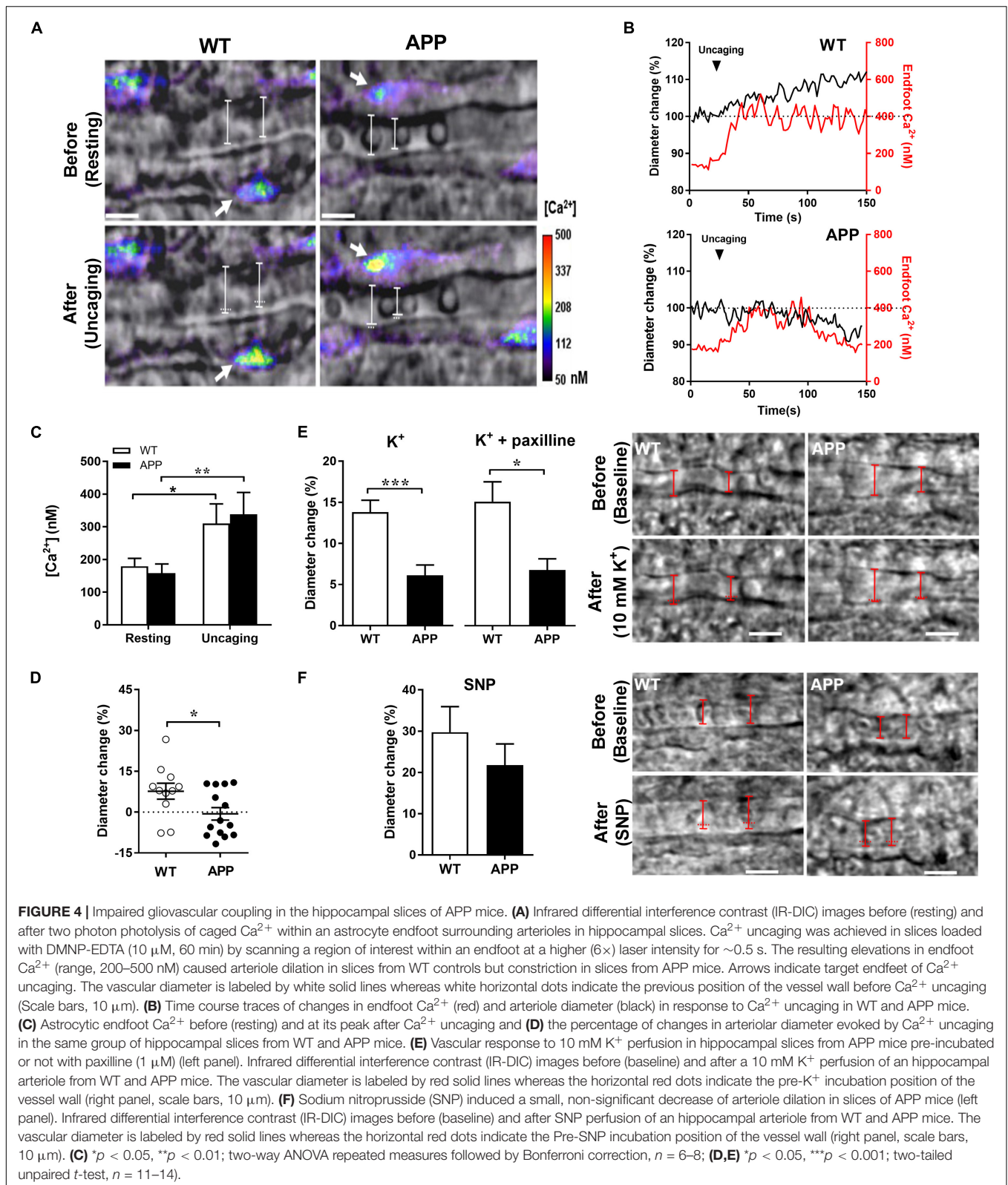
We then verified whether endfoot Ca^{2+} uncaging increases astrocytic endfoot ROS levels and, if so, whether it correlates with the amplitude of vascular responses. As shown in **Figure 6A**, astrocytic endfoot ROS levels were increased following Ca^{2+} uncaging but more importantly in APP mice compared with WT littermates while the resting levels of ROS in astrocytic endfeet were similar between WT and APP mice (**Figure 6B**, $p < 0.05$). The dilatatory response in APP mice was significantly reduced (**Figure 6C**, $p < 0.05$).

We further pre-incubated brain slices with Tempol, a superoxide dismutase mimetic, to prevent ROS production induced by Ca^{2+} uncaging. Notably, ROS elevation observed in APP mice was significantly reduced to levels comparable to those of WT mice in the presence of Tempol, while Tempol did not further decrease ROS in WT mice (**Figure 6D**).

Tempol reversed the polarity of the vascular responses to Ca^{2+} uncaging in APP mice from a tendency to constriction to a small dilation (**Figure 6D**, $p < 0.05$, $p < 0.01$). In order to exclude a potential effect of laser Ca^{2+} uncaging damage to astrocytic endfeet and to induce a more physiological stimulation of vascular response, we tested the effect of Tempol on EFS induced vascular responses. Tempol normalized the vascular response to EFS and the duration of astrocytic endfoot Ca^{2+} elevations in APP mice (**Figure 6E**, $p < 0.05$). The above results confirmed that astrocytic ROS contribute to NVC impairment in APP mice.

Impaired Hippocampal Synaptic and Vascular Function in APP Mice

To determine whether synaptic transmission was also disturbed at the level of the Schaffer collaterals-CA1 pathway, fractional changes in excitatory postsynaptic potential (EPSP) were plotted against stimulation intensities. The input-output curve



revealed that the EPSP in APP mice was significantly lower between 0.5 and 1.2 mA (Figure 7A, $p < 0.05$, $p < 0.01$). The paired-pulse ratio (PPR), a form of calcium-dependent

short term plasticity, with interpulse interval (IPI) ranging from 50 to 200 ms was measured to analyze the potential for presynaptic glutamate release. The value of IPI between

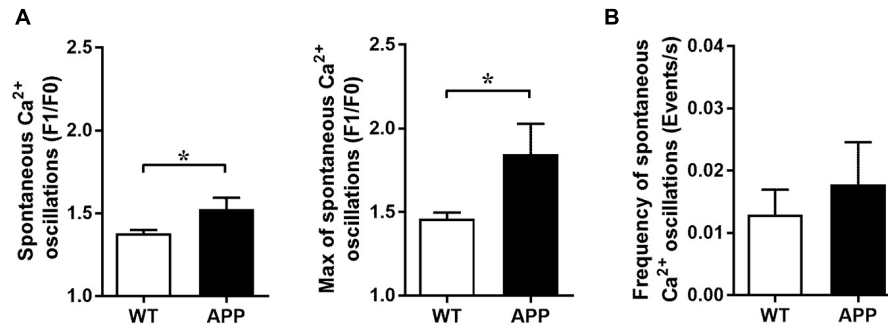


FIGURE 5 | Increased amplitude of spontaneous Ca²⁺ oscillations in astrocytic endfeet of APP mice. **(A)** Averaged (left panel) and maximal amplitude (right panel) and **(B)** frequency of spontaneous Ca²⁺ oscillations in astrocytic endfeet of hippocampal slices from WT and APP mice (**p* < 0.05; two-tailed unpaired *t*-test; *n* = 4–13). F1/F0: fractional fluorescence.

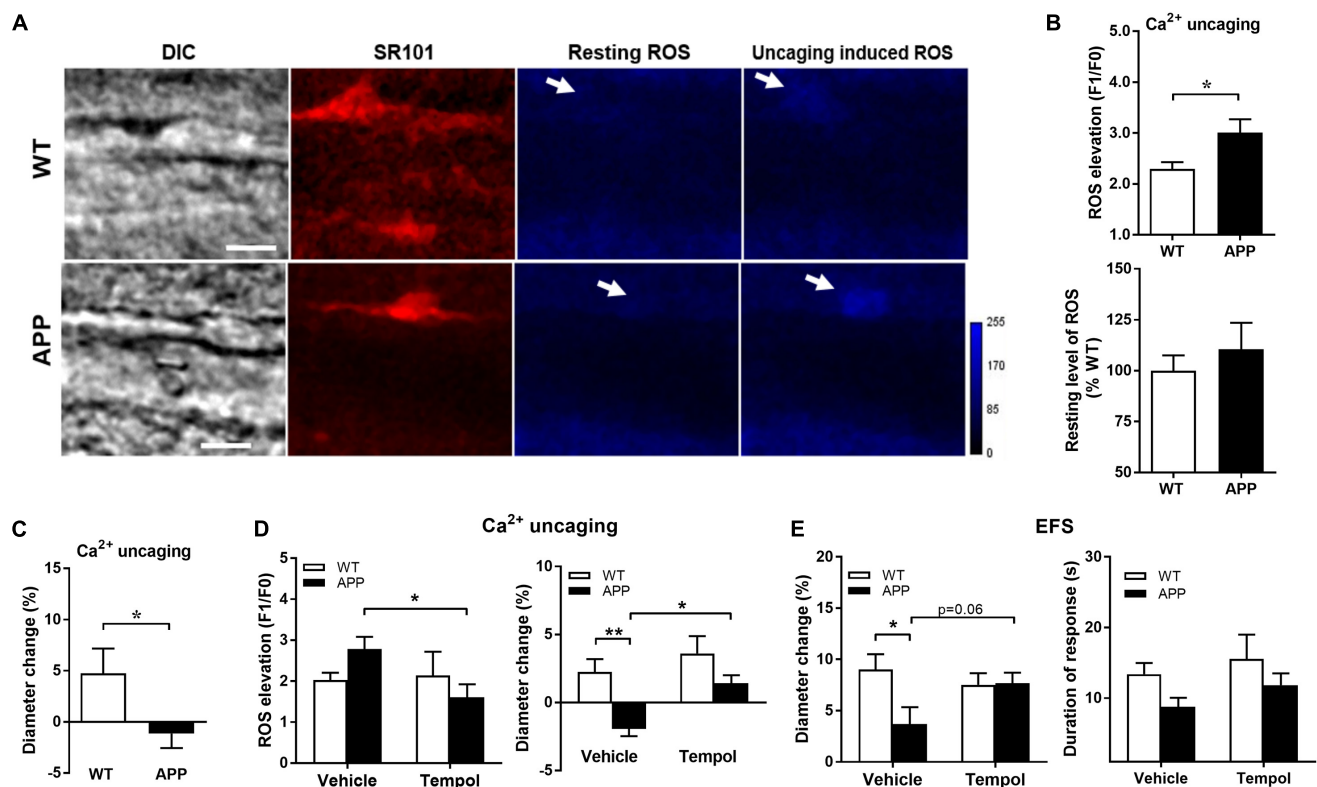
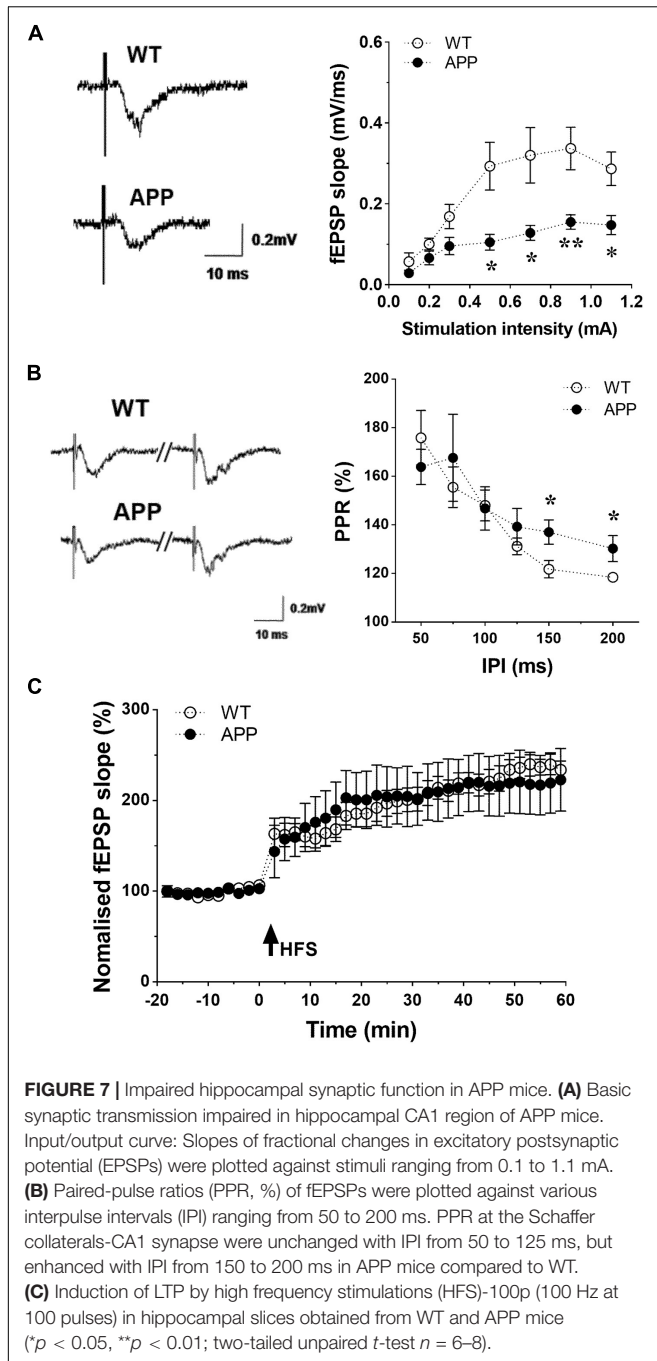


FIGURE 6 | Ca²⁺ uncaging induces a higher level of ROS production in astrocytic endfeet in APP mice. **(A)** Representative images of infrared differential interference contrast (IR-DIC), SR101 (astrocytes), resting ROS and Ca²⁺ uncaging induced ROS in brain slices from WT and APP mice. Arrows indicate targeted endfeet of Ca²⁺ uncaging (Scale bars, 10 μ m). **(B)** Astrocytic endfeet ROS production and **(C)** vascular diameter after Ca²⁺ uncaging in hippocampal slices from APP mice compared with WT (**p* < 0.05; two-tailed unpaired *t*-test; *n* = 12–16). **(D)** Tempol, through reducing the Ca²⁺ uncaging-induced astrocytic ROS production (left panel), prevented the impaired vascular response to Ca²⁺ uncaging (right panel) in APP mice (**p* < 0.05; ***p* < 0.01; two-way ANOVA followed by Bonferroni correction, *n* = 9–15). **(E)** Tempol also prevented the reduced vascular responses to EFS (left panel) without modifying the duration of the response (right panel) (**p* < 0.05; two-way ANOVA followed by Bonferroni correction, *n* = 9–15).

50 and 125 ms did not differ between APP and WT mice (Figure 7B, *p* < 0.05). However, at IPI from 150 to 200 ms, the PPR was significant higher in APP mice compared to their WT littermates, indicating a prolonged increased pre-synaptic glutamate release. The induction of Schaffer collaterals-CA1 LTP was examined by delivering a

conditioning stimulation. As shown in Figure 7C, the high frequency conditioning stimulus (4 times 100 pulses at 100 Hz) induced an increase of EPSP of approximately 110% lasting over 60 min in hippocampal slices from both APP and WT mice. Interestingly, we found that APP mice could be divided into two subgroups with 4–6 mice showing an impaired LTP



in 60 min after HFS while the rest showed improved LTP (results not shown).

DISCUSSION

This study shows, for the first time, specific impairments of hippocampal neuroglial communications in APP mice. We demonstrated that, in APP mice compared to WT controls, (i) the *in vivo* CBF increase in response to Schaffer collaterals stimulation is reduced, and (ii) the *ex vivo* vasodilation in

response to neuronal stimulation or astrocytic Ca^{2+} elevation is also diminished. These observations may be explained, at least in part, by an attenuated fEPSP slope and PPR, shorter astrocytic endfoot Ca^{2+} increases and a decreased vascular reactivity to K^+ . Scavenging ROS with Tempol in APP mice normalized the vascular responses to neuronal stimulation and astrocytic Ca^{2+} elevations.

While many studies have investigated NVC in the somatosensory cortex (Park et al., 2004, 2020; Ongali et al., 2010; Duncombe et al., 2017; Royea et al., 2020) of APP mice, the present study establishes, both *in vivo* and *ex vivo*, that NVC is also impaired in the hippocampus of APP mice. Considering that, in human, $\text{A}\beta$ deposition occurs mainly in the entorhinal cortex and hippocampus (Ulrich, 1985; Vogel et al., 2021), it is crucial to understand the mechanisms leading to neurodegeneration in these regions. In the present study, APP J20 mice expressed both the human APP familial Swedish and Indiana mutations and are characterized by the presence of $\text{A}\beta$ plaques in the hippocampus at 6 months of age (Aucoin et al., 2005). We also confirmed the presence of $\text{A}\beta$ plaques in the vicinity of astrocytes and blood vessels of the hippocampus.

NVC is, at least partially, dependent on astrocytic Ca^{2+} rises following neuronal activation (Zonta et al., 2003a; Filosa et al., 2004; Mulligan and MacVicar, 2004; Mishra et al., 2016; Gu et al., 2018). In the present study, we observed an increased amplitude of spontaneous Ca^{2+} oscillations in astrocytic endfeet with a shorter duration of astrocytic Ca^{2+} elevations in response to EFS. Increased in spontaneous astrocytic Ca^{2+} activity has also been reported in APP/PS1 mice (Kuchibhotla et al., 2009).

This increase in spontaneous activity seems to be independent of changes in neuronal activity (Kuchibhotla et al., 2009). Actually, acute or chronic exposure of isolated astrocytes to $\text{A}\beta$ has been shown to enhance spontaneous intracellular Ca^{2+} transient signaling (Haughey and Mattson, 2003; Lim et al., 2013; Alberdi et al., 2013; Lee et al., 2014). This increase in Ca^{2+} partially originates from intracellular sources such as the endoplasmic reticulum (Toivari et al., 2011). In addition, $\text{A}\beta$ interacts with several types of receptors in astrocytes leading to Ca^{2+} entry. These receptors include the purinergic receptor P2Y1 (Delekate et al., 2014), nicotinic receptors ($\alpha 7$ -nAChRs) (Xiu et al., 2005; Lee et al., 2014) and glutamate metabotropic receptors (mGluR) (Grolla et al., 2013; Ronco et al., 2014).

The increased amplitude of spontaneous astrocytic Ca^{2+} may be responsible for the decreased duration of astrocytic Ca^{2+} elevations in response to neuronal activation. Indeed, since cytoplasmic Ca^{2+} regulation of inositol 1,4,5-trisphosphate receptors (IP_3Rs) is biphasic (Bezprozvanny et al., 1991; Foskett et al., 2007), relatively high resting $[\text{Ca}^{2+}]$ may dampen the amplitude and/or the duration of the IP_3Rs -dependent astroglial $[\text{Ca}^{2+}]$ increases. The decreased duration of astrocytic Ca^{2+} elevations in response to neuronal activation may also result from a decreased rate of exocytosis and fraction of released vesicles, as was observed in APP mice. Indeed, these parameters are known to correlate with Ca^{2+} mobilization in cultured astroglia (Kreft et al., 2004; Pryazhnikov and Khiroug, 2008). In turn, decreased duration of astrocytic Ca^{2+} elevations may have an impact on

synaptic function (gliotransmitter release, synaptic plasticity, and integrity) (Min and Nevian, 2012).

Resting astrocytic Ca^{2+} controls tonic vasodilation independently of neuronal activity (Rosenegger et al., 2015). However, in the present study, the vascular tone does not seem to differ between WT and APP mice since the level of precontraction induced by a thromboxane receptor agonist was the same in these groups (Blanco et al., 2008). The link between spatiotemporal characteristics of astrocytic Ca^{2+} increases and the amplitude and duration of the vascular response remains to be further investigated (Sharma et al., 2020).

To better understand how the gliovascular communication is impacted in APP mice, Ca^{2+} was uncaged in the astrocytic endfeet to induce comparable Ca^{2+} increases. Interestingly, the vascular responses to Ca^{2+} uncaging was shifted toward constriction or smaller dilations in APP mice compared with WT controls suggesting a change in vascular reactivity to astrocytic-derived vasomediators. Astrocytic Ca^{2+} increases induce the release of various vasoactive molecules (Girouard and Iadecola, 2006). These include arachidonic acid metabolites such as prostaglandin E2 (PGE2) (Zonta et al., 2003b; Takano et al., 2006; Gordon et al., 2008; Mishra et al., 2011; Hall et al., 2014) and epoxyeicosatrienoic acids (EETs) (Alkayed et al., 1997; Metea and Newman, 2006b), ions such as K^+ (Filosa et al., 2004), and metabolic by-products such as lactate (Gordon et al., 2008) and adenosine (Xu and Pelligrino, 2007; Vetri et al., 2011). Astrocytes could also release arachidonic acid which is metabolized into the vasoconstrictor hydroxyeicosatetraenoic acid (20-HETE) in vascular smooth muscle cells (Mulligan and MacVicar, 2004; Metea and Newman, 2006a; Mishra et al., 2011; Hall et al., 2014). Since K^+ exerts a biphasic effect on vascular responses, low concentrations leading to dilation and higher concentrations causing constriction, we hypothesized that astrocytes in APP mice may release more K^+ . However, the selective BK-channel blocker, paxilline did not modify the vascular response to K^+ , while the vascular responses to K^+ alone are attenuated. This effect seems to be specific to K^+ since vascular responses to the NO donor, SNP, or the thromboxane A_2 receptor agonist, U46619 did not differ between WT and APP mice. These results suggest that the inward rectifier K^+ (K_{ir}) channels may be altered in APP mice. Indeed, it was demonstrated that impairment in NVC in a mouse model of familial AD (5xFAD) is attributable to reduced activity of capillary $\text{K}_{\text{ir}}2.1$ channels (Mughal et al., 2021). K_{ir} channel function was also altered in cerebrovascular endothelial cells of the triple transgenic AD model (mutations in the PS1, APP, and tau genes) (Hakim and Behringer, 2020). Capillaries $\text{K}_{\text{ir}}2.1$ channels are involved in NVC by translating local elevation of K^+ into upstream arteriolar dilations (Longden et al., 2017). Overall, these data suggest that the K_{ir} channel-dependent vascular response to astrocyte-derived K^+ is impaired in APP mice. However, this does not exclude the possibility of a change in the concentration or nature of vasomediators derived from astrocytes.

Using the superoxide anion mimetic, Tempol, we demonstrated that ROS are involved in the impaired vascular responses to neuronal and astrocytic activation but not in the decreased duration of astrocytic Ca^{2+} responses to neuronal

activity. The impact of ROS on NVC had been demonstrated in many models. In APP mice, it was demonstrated that cerebrovascular oxidative stress originates from the action of $\text{A}\beta$ peptide on the innate immunity receptor CD36 on perivascular macrophages, which in turn, activates a Nox2-containing NADPH oxidase. This $\text{A}\beta$ -induced vascular oxidative stress resulted in impaired NVC (Tong et al., 2009; Park et al., 2017) and endothelial-dependent dilatory function (Zhang et al., 2013). Nevertheless, although it had been suggested that ROS may block or knockdown $\text{K}_{\text{ir}}2.1$ channels (Zhang et al., 2019), the cause-effect relationship between ROS and impaired K_{ir} vascular dependent responses in APP mice remains to be established.

In conclusion, we have demonstrated that hippocampal NVC is altered at many levels of the neurovascular unit in APP mice and that an acute antioxidant treatment normalizes NVC as well as the vascular response to astrocytic Ca^{2+} pathway activation. These data support the inclusion of antioxidants in therapies aiming to preserve the neurovascular unit in AD.

DATA AVAILABILITY STATEMENT

The original contributions presented in the study are included in the article/**Supplementary Material**, further inquiries can be directed to the corresponding author/s.

ETHICS STATEMENT

The animal study was reviewed and approved by the Canadian Council on Animal Care, Committee on Ethics of Animal Experiments and Animal Research: Reporting of *in vivo* Experiments of the Université de Montréal and the Montreal Neurological Institute at McGill University.

AUTHOR CONTRIBUTIONS

LL, X-KT, EH, and HG contributed to conception and design of the study. LL, X-KT, and DV performed the research. LL, X-KT, DV, and HG analyzed the data. LL, X-KT, MH, DV, and HG wrote the manuscript. All authors contributed to the article and approved the submitted version.

FUNDING

This study was supported by grants (EH and HG) from the Fonds de Recherche du Québec-Santé—National Natural Science Foundation of China (FRQS-NSFC) Collaboration “Research Program on Aging,” the Canadian Institutes of Health Research (EH, CIHR MOP-12600 and HG, CIHR MOP-175046).

ACKNOWLEDGMENTS

We would like to acknowledge Ms. Jessika Royea from the Hamel’s lab for APP mouse preparation and Louis-Eric Trudeau (Department of Pharmacology and Physiology,

Université de Montréal) for providing electrophysiological experimental platform. We would like to thank Lennart Mucke from the Gladstone Institute of Neurological Disease and Department of Neurology, University of California, San Francisco, CA, for providing the APP mouse breeders.

REFERENCES

- Abramov, A. Y., Canevari, L., and Duchen, M. R. (2004). Beta-amyloid peptides induce mitochondrial dysfunction and oxidative stress in astrocytes and death of neurons through activation of NADPH oxidase. *J. Neurosci.* 24, 565–575. doi: 10.1523/jneurosci.4042-03.2004
- Alberdi, E., Wyssenbach, A., Alberdi, M., Sanchez-Gomez, M. V., Cavaliere, F., Rodriguez, J. J., et al. (2013). Ca(2+)-dependent endoplasmic reticulum stress correlates with astrogliosis in oligomeric amyloid beta-treated astrocytes and in a model of Alzheimer's disease. *Aging Cell* 12, 292–302. doi: 10.1111/acel.12054
- Alkayed, N. J., Birks, E. K., Narayanan, J., Petrie, K. A., Kohler-Cabot, A. E., and Harder, D. R. (1997). Role of P-450 arachidonic acid epoxygenase in the response of cerebral blood flow to glutamate in rats. *Stroke* 28, 1066–1072. doi: 10.1161/01.str.28.5.1066
- Aucoin, J. S., Jiang, P., Aznavour, N., Tong, X. K., Buttini, M., Descarries, L., et al. (2005). Selective cholinergic denervation, independent from oxidative stress, in a mouse model of Alzheimer's disease. *Neuroscience* 132, 73–86. doi: 10.1016/j.neuroscience.2004.11.047
- Bailey, T. L., Rivara, C. B., Rocher, A. B., and Hof, P. R. (2004). The nature and effects of cortical microvascular pathology in aging and Alzheimer's disease. *Neurol. Res.* 26, 573–578. doi: 10.1179/016164104225016272
- Bezprozvanny, I., Watras, J., and Ehrlich, B. E. (1991). Bell-shaped calcium-response curves of Ins(1,4,5)P₃- and calcium-gated channels from endoplasmic reticulum of cerebellum. *Nature* 351, 751–754. doi: 10.1038/351751a0
- Blanco, V. M., Stern, J. E., and Filosa, J. A. (2008). Tone-dependent vascular responses to astrocyte-derived signals. *Am. J. Physiol. Heart Circ. Physiol.* 294, H2855–H2863.
- Delekate, A., Fuchtemeier, M., Schumacher, T., Ulbrich, C., Foddiss, M., and Petzold, G. C. (2014). Metabotropic P2Y₁ receptor signalling mediates astrocytic hyperactivity in vivo in an Alzheimer's disease mouse model. *Nat. Commun.* 5:5422.
- Duncombe, J., Lennen, R. J., Jansen, M. A., Marshall, I., Wardlaw, J. M., and Horsburgh, K. (2017). Ageing causes prominent neurovascular dysfunction associated with loss of astrocytic contacts and gliosis. *Neuropathol. Appl. Neurobiol.* 43, 477–491. doi: 10.1111/nan.12375
- Filosa, J. A., Bonev, A. D., and Nelson, M. T. (2004). Calcium dynamics in cortical astrocytes and arterioles during neurovascular coupling. *Circ. Res.* 95, e73–e81.
- Foskett, J. K., White, C., Cheung, K. H., and Mak, D. O. (2007). Inositol trisphosphate receptor Ca²⁺ release channels. *Physiol. Rev.* 87, 593–658. doi: 10.1152/physrev.00035.2006
- Franklin, K. B. J., and Paxinos, G. (1997). *The Mouse Brain in Stereotaxic Coordinates*. San Diego, CA: Academic Press. doi: 10.1111/j.1469-7580.2004.00264.x
- Girouard, H., Bonev, A. D., Hannah, R. M., Meredith, A., Aldrich, R. W., and Nelson, M. T. (2010). Astrocytic endfoot Ca²⁺ and BK channels determine both arteriolar dilation and constriction. *Proc. Natl. Acad. Sci. U.S.A.* 107, 3811–3816. doi: 10.1073/pnas.0914722107
- Girouard, H., and Iadecola, C. (2006). Neurovascular coupling in the normal brain and in hypertension, stroke, and Alzheimer disease. *J. Appl. Physiol.* 100, 328–335. doi: 10.1152/jappphysiol.00966.2005
- Gordon, G. R., Choi, H. B., Rungta, R. L., Ellis-Davies, G. C., and MacVicar, B. A. (2008). Brain metabolism dictates the polarity of astrocyte control over arterioles. *Nature* 456, 745–749. doi: 10.1038/nature07525
- Grolla, A. A., Sim, J. A., Lim, D., Rodriguez, J. J., Genazzani, A. A., and Verkhratsky, A. (2013). Amyloid-beta and Alzheimer's disease type pathology differentially affects the calcium signalling toolkit in astrocytes from different brain regions. *Cell Death Dis.* 4:e623. doi: 10.1038/cddis.2013.145
- Gu, X., Chen, W., Volkow, N. D., Koretsky, A. P., Du, C., and Pan, Y. (2018). Synchronized astrocytic Ca(2+) responses in neurovascular coupling during somatosensory stimulation and for the resting state. *Cell Rep.* 23, 3878–3890. doi: 10.1016/j.celrep.2018.05.091
- Hakim, M. A., and Behringer, E. J. (2020). Development of Alzheimer's disease progressively alters sex-dependent K_{Ca} and sex-independent K_{IR} channel function in cerebrovascular endothelium. *J. Alzheimers Dis.* 76, 1423–1442. doi: 10.3233/jad-200085
- Hall, C. N., Reynell, C., Gesslein, B., Hamilton, N. B., Mishra, A., Sutherland, B. A., et al. (2014). Capillary pericytes regulate cerebral blood flow in health and disease. *Nature* 508, 55–60. doi: 10.1038/nature13165
- Haughey, N. J., and Mattson, M. P. (2003). Alzheimer's amyloid beta-peptide enhances ATP/gap junction-mediated calcium-wave propagation in astrocytes. *Neuromol. Med.* 3, 173–180. doi: 10.1385/nmm:3:3:173
- Hock, C., Villringer, K., Muller-Spahn, F., Wenzel, R., Heekeren, H., Schuh-Hofer, S., et al. (1997). Decrease in parietal cerebral hemoglobin oxygenation during performance of a verbal fluency task in patients with Alzheimer's disease monitored by means of near-infrared spectroscopy (NIRS)—correlation with simultaneous rCBF-PET measurements. *Brain Res.* 755, 293–303. doi: 10.1016/s0006-8993(97)00122-4
- Iadecola, C. (2004). Neurovascular regulation in the normal brain and in Alzheimer's disease. *Nat. Rev. Neurosci.* 5, 347–360. doi: 10.1038/nrn1387
- Iadecola, C. (2010). The overlap between neurodegenerative and vascular factors in the pathogenesis of dementia. *Acta Neuropathol.* 120, 287–296. doi: 10.1007/s00401-010-0718-6
- Jack, C. R. Jr., Bennett, D. A., Blennow, K., Carrillo, M. C., Dunn, B., Haeberlein, S. B., et al. (2018). NIA-AA research framework: toward a biological definition of Alzheimer's disease. *Alzheimers Dement.* 14, 535–562. doi: 10.1016/j.jalz.2018.02.018
- Kreft, M., Stenovec, M., Rupnik, M., Grilc, S., Krzan, M., Potokar, M., et al. (2004). Properties of Ca(2+)-dependent exocytosis in cultured astrocytes. *Glia* 46, 437–445. doi: 10.1002/glia.20018
- Kuchibhotla, K. V., Lattarulo, C. R., Hyman, B. T., and Bacskaï, B. J. (2009). Synchronous hyperactivity and intercellular calcium waves in astrocytes in Alzheimer mice. *Science* 323, 1211–1215. doi: 10.1126/science.1169096
- Lee, L., Kosuri, P., and Arancio, O. (2014). Picomolar amyloid-beta peptides enhance spontaneous astrocyte calcium transients. *J. Alzheimers Dis.* 38, 49–62. doi: 10.3233/jad-130740
- Li, J., Wang, Y. J., Zhang, M., Xu, Z. Q., Gao, C. Y., Fang, C. Q., et al. (2011). Vascular risk factors promote conversion from mild cognitive impairment to Alzheimer disease. *Neurology* 76, 1485–1491. doi: 10.1212/wnl.0b013e318217e7a4
- Lim, D., Iyer, A., Ronco, V., Grolla, A. A., Canonico, P. L., Aronica, E., et al. (2013). Amyloid beta deregulates astroglial mGluR5-mediated calcium signaling via calcineurin and Nf-kB. *Glia* 61, 1134–1145. doi: 10.1002/glia.22502
- Longden, T. A., Dabertrand, F., Koide, M., Gonzales, A. L., Tykocki, N. R., Brayden, J. E., et al. (2017). Capillary K(+) sensing initiates retrograde hyperpolarization to increase local cerebral blood flow. *Nat. Neurosci.* 20, 717–726. doi: 10.1038/nn.4533
- Lourenço, C. F., Ledo, A., Barbosa, R. M., and Laranjinha, J. (2017). Neurovascular uncoupling in the triple transgenic model of Alzheimer's disease: impaired cerebral blood flow response to neuronal-derived nitric oxide signaling. *Exp. Neurol.* 291, 36–43. doi: 10.1016/j.expneurol.2017.01.013
- Maravall, M., Mainen, Z. F., Sabatini, B. L., and Svoboda, K. (2000). Estimating intracellular calcium concentrations and buffering without wavelength ratioing. *Biophys. J.* 78, 2655–2667. doi: 10.1016/s0006-3495(00)76809-3
- Metea, M. R., and Newman, E. A. (2006b). Glial cells dilate and constrict blood vessels: a mechanism of neurovascular coupling. *J. Neurosci.* 26, 2862–2870. doi: 10.1523/jneurosci.4048-05.2006
- Metea, M. R., and Newman, E. A. (2006a). Calcium signaling in specialized glial cells. *Glia* 54, 650–655. doi: 10.1002/glia.20352

SUPPLEMENTARY MATERIAL

The Supplementary Material for this article can be found online at: <https://www.frontiersin.org/articles/10.3389/fphys.2021.715446/full#supplementary-material>

- Min, R., and Nevian, T. (2012). Astrocyte signaling controls spike timing-dependent depression at neocortical synapses. *Nat. Neurosci.* 15, 746–753. doi: 10.1038/nn.3075
- Mishra, A., Hamid, A., and Newman, E. A. (2011). Oxygen modulation of neurovascular coupling in the retina. *Proc. Natl. Acad. Sci. U.S.A.* 108, 17827–17831. doi: 10.1073/pnas.1110533108
- Mishra, A., Reynolds, J. P., Chen, Y., Gourine, A. V., Rusakov, D. A., and Attwell, D. (2016). Astrocytes mediate neurovascular signaling to capillary pericytes but not to arterioles. *Nat. Neurosci.* 19, 1619–1627. doi: 10.1038/nn.4428
- Mucke, L., Masliah, E., Yu, G. Q., Mallory, M., Rockenstein, E. M., Tatsuno, G., et al. (2000). High-level neuronal expression of abeta 1-42 in wild-type human amyloid protein precursor transgenic mice: synaptotoxicity without plaque formation. *J. Neurosci.* 20, 4050–4058. doi: 10.1523/jneurosci.20-11-04050.2000
- Mughal, A., Harraz, O. F., Gonzales, A. L., Hill-Eubanks, D., and Nelson, M. T. (2021). PIP2 improves cerebral blood flow in a mouse model of Alzheimer's disease. *Function (Oxf.)* 2:zqab010.
- Mulligan, S. J., and MacVicar, B. A. (2004). Calcium transients in astrocyte endfeet cause cerebrovascular constrictions. *Nature* 431, 195–199. doi: 10.1038/nature02827
- Nicolakakis, N., Aboukassim, T., Ongali, B., Lecrux, C., Fernandes, P., Rosa-Neto, P., et al. (2008). Complete rescue of cerebrovascular function in aged Alzheimer's disease transgenic mice by antioxidants and pioglitazone, a peroxisome proliferator-activated receptor gamma agonist. *J. Neurosci.* 28, 9287–9296. doi: 10.1523/jneurosci.3348-08.2008
- Ongali, B., Nicolakakis, N., Lecrux, C., Aboukassim, T., Rosa-Neto, P., Papadopoulos, P., et al. (2010). Transgenic mice overexpressing APP and transforming growth factor-beta1 feature cognitive and vascular hallmarks of Alzheimer's disease. *Am. J. Pathol.* 177, 3071–3080. doi: 10.2353/ajpath.2010.100339
- Park, L., Anrather, J., Forster, C., Kazama, K., Carlson, G. A., and Iadecola, C. (2004). Abeta-induced vascular oxidative stress and attenuation of functional hyperemia in mouse somatosensory cortex. *J. Cereb. Blood Flow Metab.* 24, 334–342. doi: 10.1097/01.wcb.0000105800.49957.1e
- Park, L., Uekawa, K., Garcia-Bonilla, L., Koizumi, K., Murphy, M., Pistik, R., et al. (2017). Brain perivascular macrophages initiate the neurovascular dysfunction of Alzheimer Abeta peptides. *Circ. Res.* 121, 258–269. doi: 10.1161/circresaha.117.311054
- Park, L., Zhou, J., Koizumi, K., Wang, G., Anfray, A., Ahn, S. J., et al. (2020). tPA deficiency underlies neurovascular coupling dysfunction by amyloid-beta. *J. Neurosci.* 40, 8160–8173. doi: 10.1523/jneurosci.1140-20.2020
- Pryazhnikov, E., and Khiroug, L. (2008). Sub-micromolar increase in [Ca(2+)](i) triggers delayed exocytosis of ATP in cultured astrocytes. *Glia* 56, 38–49. doi: 10.1002/glia.20590
- Ronco, V., Grolla, A. A., Glasnov, T. N., Canonico, P. L., Verkhatsky, A., Genazzani, A. A., et al. (2014). Differential deregulation of astrocytic calcium signalling by amyloid-beta, TNFalpha, IL-1beta and LPS. *Cell Calcium* 55, 219–229. doi: 10.1016/j.ceca.2014.02.016
- Rosenegger, D. G., Tran, C. H., Wamsteeker Cusulin, J. I., and Gordon, G. R. (2015). Tonic local brain blood flow control by astrocytes independent of phasic neurovascular coupling. *J. Neurosci.* 35, 13463–13474. doi: 10.1523/jneurosci.1780-15.2015
- Royea, J., Martinot, P., and Hamel, E. (2020). Memory and cerebrovascular deficits recovered following angiotensin IV intervention in a mouse model of Alzheimer's disease. *Neurobiol. Dis.* 134, 104644. doi: 10.1016/j.nbd.2019.104644
- Sharma, K., Gordon, G. R. J., and Tran, C. H. T. (2020). Heterogeneity of sensory-induced astrocytic Ca(2+) dynamics during functional hyperemia. *Front. Physiol.* 11:611884. doi: 10.3389/fphys.2020.611884
- Takano, T., Han, X., Deane, R., Zlokovic, B., and Nedergaard, M. (2007). Two-photon imaging of astrocytic Ca²⁺ signaling and the microvasculature in experimental mice models of Alzheimer's disease. *Ann. N. Y. Acad. Sci.* 1097, 40–50. doi: 10.1196/annals.1379.004
- Takano, T., Tian, G. F., Peng, W., Lou, N., Libionka, W., Han, X., et al. (2006). Astrocyte-mediated control of cerebral blood flow. *Nat. Neurosci.* 9, 260–267. doi: 10.1038/nn1623
- Toivari, E., Manninen, T., Nahata, A. K., Jalonen, T. O., and Linne, M. L. (2011). Effects of transmitters and amyloid-beta peptide on calcium signals in rat cortical astrocytes: Fura-2AM measurements and stochastic model simulations. *PLoS One* 6:e17914. doi: 10.1371/journal.pone.0017914
- Tong, X. K., Lecrux, C., Rosa-Neto, P., and Hamel, E. (2012). Age- and memory rescue by simvastatin of Alzheimer's disease cerebrovascular and memory deficits. *J. Neurosci.* 32, 4705–4715. doi: 10.1523/jneurosci.0169-12.2012
- Tong, X. K., Nicolakakis, N., Fernandes, P., Ongali, B., Brouillette, J., Quirion, R., et al. (2009). Simvastatin improves cerebrovascular function and counters soluble amyloid-beta, inflammation and oxidative stress in aged APP mice. *Neurobiol. Dis.* 35, 406–414. doi: 10.1016/j.nbd.2009.06.003
- Ulrich, J. (1985). Alzheimer changes in nondemented patients younger than sixty-five: possible early stages of Alzheimer's disease and senile dementia of Alzheimer type. *Ann. Neurol.* 17, 273–277. doi: 10.1002/ana.410170309
- Vetri, F., Xu, H., Mao, L., Paisansathan, C., and Pelligrino, D. A. (2011). ATP hydrolysis pathways and their contributions to pial arteriolar dilation in rats. *Am. J. Physiol. Heart Circ. Physiol.* 301, H1369–H1377.
- Vogel, J. W., Young, A. L., Oxtoby, N. P., Smith, R., Ossenkoppe, R., Strandberg, O. T., et al. (2021). Four distinct trajectories of tau deposition identified in Alzheimer's disease. *Nat. Med.* 27, 871–881. doi: 10.1038/s41591-021-01309-6
- Xiu, J., Nordberg, A., Zhang, J. T., and Guan, Z. Z. (2005). Expression of nicotinic receptors on primary cultures of rat astrocytes and up-regulation of the alpha7, alpha4 and beta2 subunits in response to nanomolar concentrations of the beta-amyloid peptide(1-42). *Neurochem. Int.* 47, 281–290. doi: 10.1016/j.neuint.2005.04.023
- Xu, H. L., and Pelligrino, D. A. (2007). ATP release and hydrolysis contribute to rat pial arteriolar dilatation elicited by neuronal activation. *Exp. Physiol.* 92, 647–651. doi: 10.1113/expphysiol.2006.036863
- Yetkin, F. Z., Rosenberg, R. N., Weiner, M. F., Purdy, P. D., and Cullum, C. M. (2006). FMRI of working memory in patients with mild cognitive impairment and probable Alzheimer's disease. *Europ. Radiol.* 16, 193–206. doi: 10.1007/s00330-005-2794-x
- Zhang, L., Papadopoulos, P., and Hamel, E. (2013). Endothelial TRPV4 channels mediate dilation of cerebral arteries: impairment and recovery in cerebrovascular pathologies related to Alzheimer's disease. *Br. J. Pharmacol.* 170, 661–670. doi: 10.1111/bph.12315
- Zhang, X., Cui, X., Li, X., Yan, H., Li, H., Guan, X., et al. (2019). Inhibition of Kir2.1 channel-induced depolarization promotes cell biological activity and differentiation by modulating autophagy in late endothelial progenitor cells. *J. Mol. Cell. Cardiol.* 127, 57–66. doi: 10.1016/j.yjmcc.2018.11.005
- Zlokovic, B. V. (2011). Neurovascular pathways to neurodegeneration in Alzheimer's disease and other disorders. *Nat. Rev. Neurosci.* 12, 723–738. doi: 10.1038/nrn3114
- Zonta, M., Angulo, M. C., Gobbo, S., Rosengarten, B., Hossmann, K. A., Pozzan, T., et al. (2003a). Neuron-to-astrocyte signaling is central to the dynamic control of brain microcirculation. *Nat. Neurosci.* 6, 43–50. doi: 10.1038/nn980
- Zonta, M., Sebelin, A., Gobbo, S., Fellin, T., Pozzan, T., and Carmignoto, G. (2003b). Glutamate-mediated cytosolic calcium oscillations regulate a pulsatile prostaglandin release from cultured rat astrocytes. *J. Physiol.* 553, 407–414. doi: 10.1113/jphysiol.2003.046706

Conflict of Interest: The authors declare that the research was conducted in the absence of any commercial or financial relationships that could be construed as a potential conflict of interest.

Publisher's Note: All claims expressed in this article are solely those of the authors and do not necessarily represent those of their affiliated organizations, or those of the publisher, the editors and the reviewers. Any product that may be evaluated in this article, or claim that may be made by its manufacturer, is not guaranteed or endorsed by the publisher.

Copyright © 2021 Li, Tong, Hosseini Kahnouei, Vallerand, Hamel and Girouard. This is an open-access article distributed under the terms of the Creative Commons Attribution License (CC BY). The use, distribution or reproduction in other forums is permitted, provided the original author(s) and the copyright owner(s) are credited and that the original publication in this journal is cited, in accordance with accepted academic practice. No use, distribution or reproduction is permitted which does not comply with these terms.